Supporting Information

Tailored charge distribution modulated by cyclic carbonate enabling high-performance PEO-based solid electrolyte

Qiuying Xu,[ab] Zunxiang Hu,[b] Yaning Shangguan,[b] Lina Liu,[b] Rongmin Lu,[b] Lijuan Zhang,[a]* Xuehui Shangguan,[b]* Lijun Gao,[c]* Mengmeng Liu,[b] Haixin Zhang,[d] Huanqi Yao,[e] Qinglei Wang,[b]* Faqiang Li,[b]*

[a]School of Chemistry and Materilals Science, Qinghai Minzu University, Xining 810007, China

[b]School of Materials Science and Engineering, Linyi University, Linyi 276003, China

[c]School of Materials Science and Engineering, Yanshan University, Qinhuangdao 066000, China

[d]Shandong Xinhai Technology Co., Ltd., Linyi 276600, China

[e]Shandong Shuaibang New Energy Co., Ltd., Linyi 276014, China

*** Correspondence:**

Lijuan Zhang, Xuehui Shangguan, Lijun Gao, Qinglei Wang, Faqiang Li
zhanglijuan2002@126.com (L. Zhang), shangguanxuehui@lyu.edu.cn (X. Shangguan), gaolj_1991@163.com (L. GaO), wangqinglei@lyu.edu.cn (Q. Wang), lifaqiang@lyu.edu.cn (F. Li).

1. Supplementary Experimental Section

1.1 Recrystallization of AIBN

After heating 100 ml anhydrous ethanol at 70~80 °C, add 10 g AIBN powder to it, wait for it to dissolve, and preheat the Brinell funnel and suction filter bottle at the same time. After the AIBN is completely dissolved, it is drained while hot, and the filtrate is placed in a small beaker and sealed with plastic wrap and placed at low temperature to recrystallize. Then, the obtained AIBN particles are placed in a surface dish and baked in a vacuum oven at 60 °C for 1 h. Subsequently, the AIBN is loaded into brown bottles and transferred to the glove box for later use.

1.2 Coin cell assembly

To prepare the composite cathode, $LiCoO_2$ (LCO, 1 C = 160 mAh g^{-1}))/$LiNi_{0.5}Co_{0.2}Mn_{0.3}O_2$ (NCM 532, 1 C = 170 mAh g^{-1})/$LiFePO_4$(LFP, 1 C = 160 mAh g^{-1})(used as an active material), super P (used as a conductive agent), and poly (vinylidene fluoride) (used as a binder) are mixed in N-methylpyrrolidone at a mass ratio of 8:1:1. The resulting paste is applied to the Al foil using a scraper coating method, then dried in a blast drying oven at 60 °C, and then transferred to a vacuum drying at 120 °C for 12 hours. After manufacturing, the electrodes are cut into 12 mm diameter discs and stored in a glove box before use. The loading of cathode active materials for LCO, LFP and NCM532 is approximately 1.5 mg cm^{-2}. SiO500 electrodes were prepared by mixing SiO500, super P and polyacrylic acid in a mass ratio of 8:1:1 in ultrapure water. The prepared slurry is cast onto Cu foils and dried at 120 °C under vacuum for more than 12 h in vacuum to prepare 14 mm diameter discs with anode loading of 1.3 mg cm^{-2} and stored in a glove box before use. A 1Ah pouch cell is used, with 3 g of electrolyte injected per Ah. The formation process includes gas release and resealing, resulting in a battery with an electrochemical window of 3 to 4.4 V. After cycling the soft-pack battery 10 times, perform folding, shearing, crushing, and needle-puncture tests at a voltage of 4.4V.

1.3 Characterization

Cycled LCO electrode morphology and microstructure are examined using scanning electron microscopy (SEM, Hitachi S4800), transmission electron microscope (TEM, FEI-TALOS-F200X) and selected area electron diffraction (SAED). The morphology of Li deposited on copper foil is observed by scanning electron microscopy (SEM, Hitachi S4800). The chemical composition of the cyclic electrode is obtained by X-ray photoelectron spectroscopy (XPS, ESCALAB 250Xi spectrometer). In-situ XRD measurements are conducted using a Rigaku Smartlab diffractometer equipped with a Cu Kα radiation source (λ = 0.154 nm). The measurements are performed in the 2θ range of 10° to 80° to analyze the crystal structures of the prepared materials during battery cycling. The in-situ battery is cycled at a rate of 0.15 C within a voltage window of 3.0-4.4 V. The battery is assembled in a coin cell configuration, consisting of an external protective casing, LCO cathode electrode, separator, lithium anode, and a spring to maintain contact during cycling. The glass transition temperature of the electrolyte is detected by differential scanning calorimetry (DSC), and the rate of 10°C min^{-1} is carried out from -80 °C to 120 °C. FTIR spectra acquired on an infrared spectrometer (Beijing Scistar Technology) underwent analysis. In situ ATR-FTIR measurements utilized an FTIR spectrometer (INVENIO S) with an extended-range Germanium ATR accessory. All spectra are collected at 16 scans per spectrum with a resolution of 4 cm^{-1}. For in situ FTIR testing of LCO cathodes, a mixture of 80% active material, 10% super P, and 10% polytetrafluoroethylene (PTFE) is pressed onto stainless steel meshes (φ16.5 mm). The in-situ optical microscopy is taken with a high-definition digital electronic measurement microscope, using a mold purchased from Beijing Scistar Technology Co, LTD. TG characterization is performed using TA Instruments Q50 TGA from ambient temperature to 800 °C at a heating rate of 10 °C min^{-1}.

1.4 Electrochemical characterization

Assembled in argon-filled glovebox with ultra-low water and oxygen levels (<0.01 ppm), CR2032 coin cells underwent testing. Each cell received 80 μL electrolyte and

underwent charge/discharge measurements at 25°C using the Neware battery testing system. The electrochemical performance of Li/SPE/LCO batteries, Li/SPE/LFP batteries and Li/SPE/NCM532 batteries are evaluated at constant current at a cutoff voltage of 3-4.4V, 2.5-4.2V and 3-4.4V (relative to Li/Li^+) using the Neware battery test system. In order to evaluate the compatibility of the electrolyte with the silicon-based negative electrode, the electrochemical performance of the SiO500/SPE/Li battery is evaluated and under constant current. The cut-off voltage of Li/graphite battery is 0.01 V-2 V, which is activated at 0.05C rate and then cycled at 0.1 C for a long time. To evaluate rate performance, Li/SPE/LCO batteries are tested at 0.1C, 0.2C, 0.3C, 0.5C, 1C, and 0.1C rates, while Li/SPE/LFP batteries are tested at 0.1C, 0.5C, 1C, 2C, 3C, and 0.1C rates, and the SiO500/SPE/Li battery at 0.02C, 0.05C, 0.1C, 0.2C, and 0.02C rates. All the test temperatures are 25±0.5 °C. The electrochemical window of prepared electrolytes is assessed using LSV, employing stainless steel (SS) as the working electrode and Li foil as both reference and counter electrodes. Li/SS battery LSV measurement at 0.5 mV/s, from 0 V to 6 V, is conducted. Cyclic voltammetry (CV) tests are performed at a scan rate of 0.04 mv/s in the range of 3-4.4V. In addition, electrochemical impedance spectroscopy (EIS) measurements are performed on all cells using the same Bio-Logic VMP 3 workstation. The frequency range of the EIS test is 0.1 Hz to 7 MHz, with a disturbance voltage of 10 mV applied. The ionic conductivity of the electrolyte is determined by performing EIS tests on stainless steel/stainless steel symmetric batteries at a variety of temperatures ranging from 25 °C to 90 °C. The high frequency semicircle region represents the Li^+ transport process through the SEI, and the intermediate frequency region represents the charge transfer process. The ionic conductivity value is calculated according to Eq (1):

$$\sigma = \frac{L}{R_0 S} \tag{1}$$

where σ represents the ionic conductivity, L represents the thickness of the electrolyte, R_0 is the Ohmic resistance, and S is the area of the stainless steel.

The Bruce-Vincent-Evans method, combined with the chronometric current method and EIS measurement, is used to test the Li/Li symmetrical battery at 25 °C to

determine the migration number of Li^+ ions. The equation Eq (2) is used to calculate:

$$t_{Li^+} = \frac{I_s(\Delta V - I_i R_i)}{I_i(\Delta V - I_s R_s)} \quad (2)$$

Where ΔV is the applied voltage, I_0 and I_{SS} are the initial and steady-state current values of the timing measurement process, respectively. R_0 and R_{SS} are charge transfer resistors before and after polarization, respectively.

For Li/Cu cells, the effective area of the Cu foil disc (diameter 1.4 cm) for Li deposition was 2.01 cm^2. CE cycling measurements were conducted in Li/Cu half cells. The Cu surface was conditioned by plating 1 mA h cm^{-2} of Li and stripping to 1 V at 0.1 mA cm^{-2}. Subsequently, a Li reservoir of 0.2 mA h cm^{-2} was plated onto Cu, followed by 10 cycles of Li plating and stripping at 0.2 mA h cm^{-2} and 0.1 mA cm^{-2}. Finally, all Li on Cu was stripped to 1 V at 0.1 mA cm^{-2}. For long-term cycling, Li/Cu cells cycled at a current density of 0.1 mA cm^{-2} at 0.2 mA h cm^{-2}, were plated with a desirable Li capacity and stripped back by using a cut-off voltage of 1 V (vs. Li/Li^+). This CE was calculated by using this Eq (3):

$$CE = \frac{(Q_S + Q_c \times n)}{(Q_p + Q_c \times n)} \quad (3)$$

where Q_s is the final stripping capacity, Q_p is the initial plating capacity, Qc is the constant plating/stripping capacity for each cycle, and n is the cycle number.

1.5 Theoretical calculations

DFT calculations are carried out using Gaussian16 software. The equilibrium state structures are optimized using the B3LYP functional with the 6–311+G (d, p) basis set. The electrostatic potential, binding energy, and the highest occupied molecular orbital (HOMO) and lowest unoccupied molecular orbital (LUMO) are analyzed. The molecules are optimized using the ESP charges after ultrafine optimization. The binding energy (Eb) between the solvent/anion and cation is defined as follows Eq (4):

$$E_b = E_{total} - E_{Li} - E_s \quad (4)$$

where E_{total} is the total energy of solvent/anion with coordinated Li, E_{Li} is the single-point energy of Li, E_s is the single-point energy of solvents/anion.

2. Supporting Figures

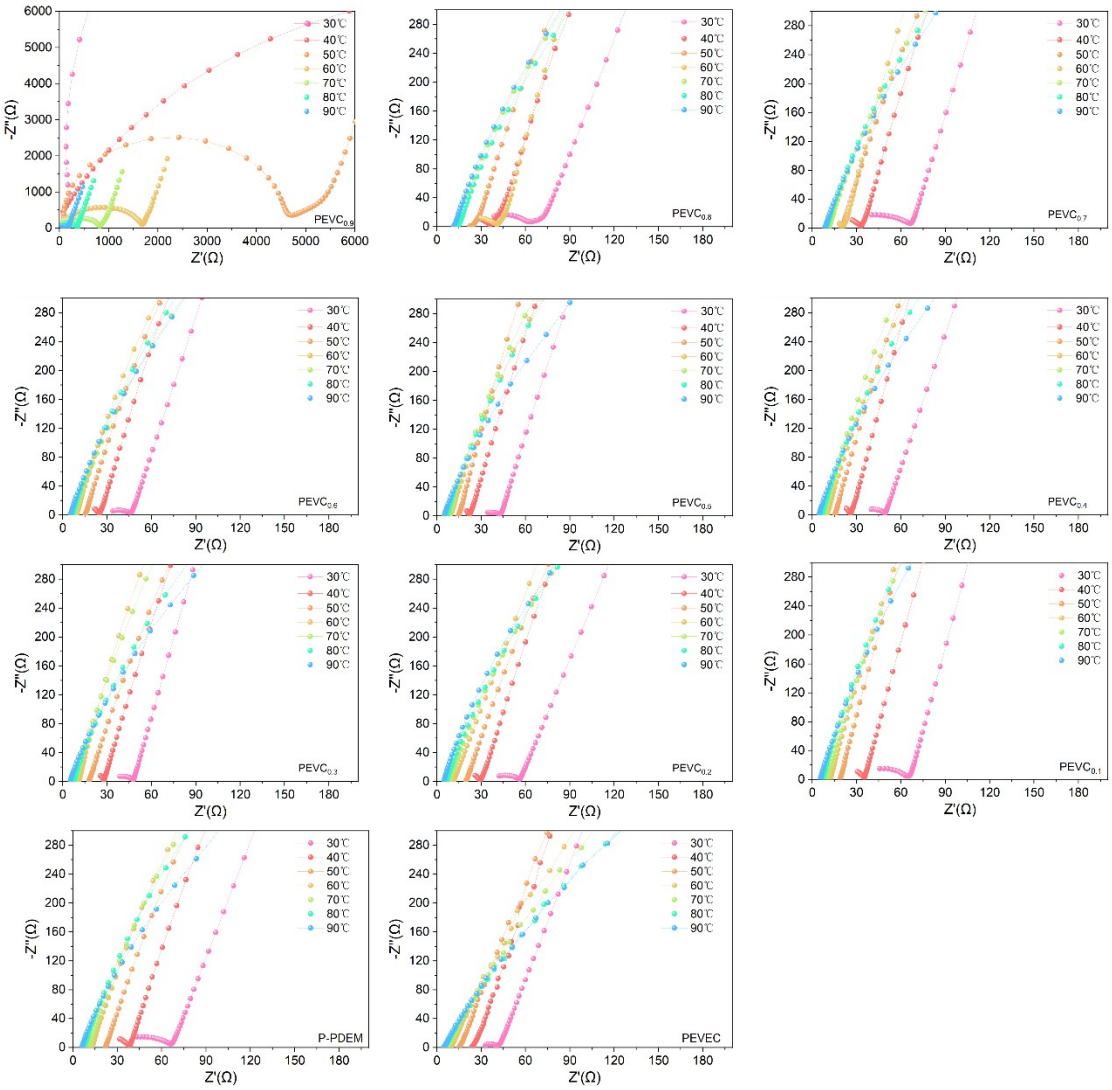

Fig.S1 Impedance spectra with different VC contents and PEVEC SPE at 30-90 °C.

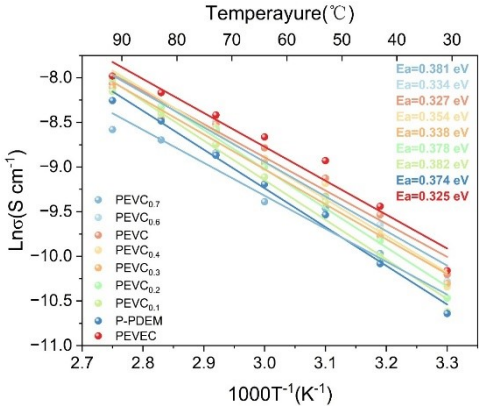

Fig.S2 Arrhenius curve with different VC content.

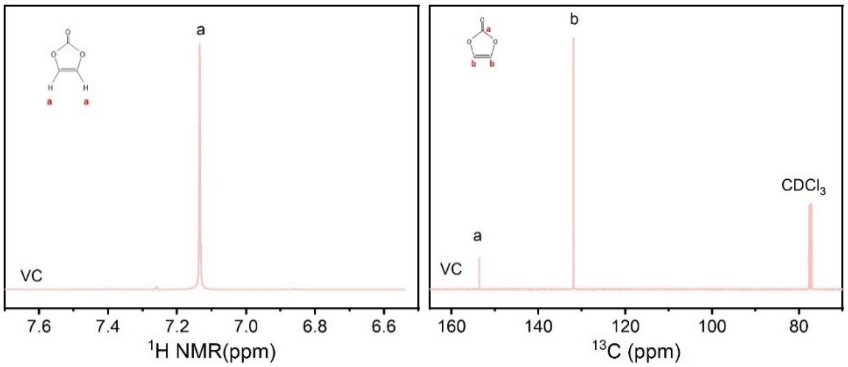

Fig.S3 The (a) ^{1}H NMR and (b) ^{13}C NMR spectrum of VC.

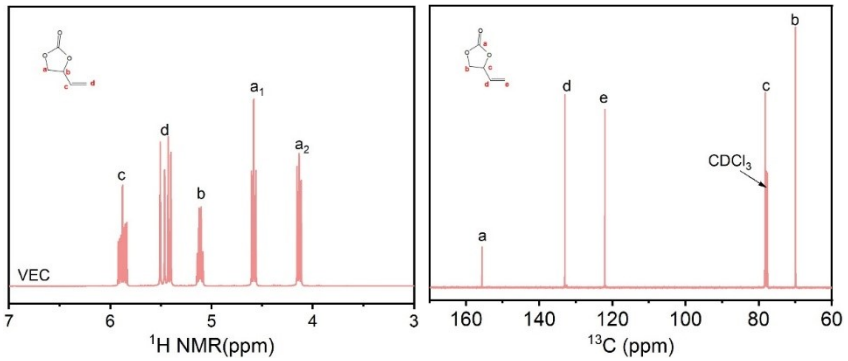

Fig.S4 The (a) ^{1}H NMR and (b) ^{13}C NMR spectrum of VEC.

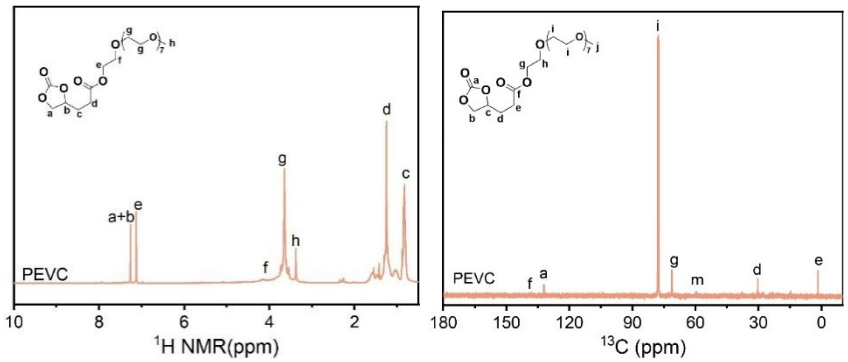

Fig.S5 The (a) ^{1}H NMR and (b) ^{13}C NMR spectrum of PEVC.

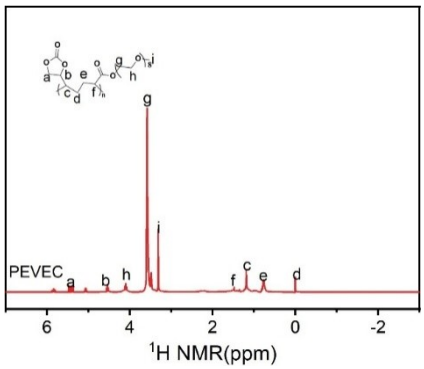

Fig.S6 The ^{1}H NMR spectrum of PEVEC.

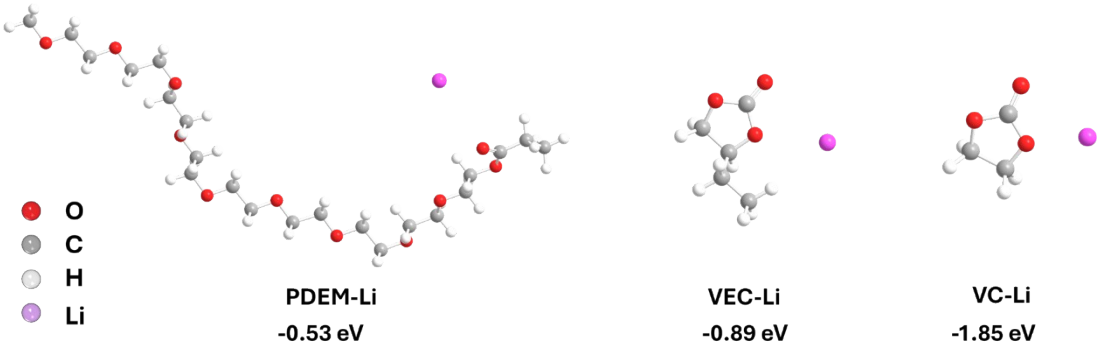

Fig.S7 Structures and binding energies of PDEM, VEC and VC calculated by DFT.

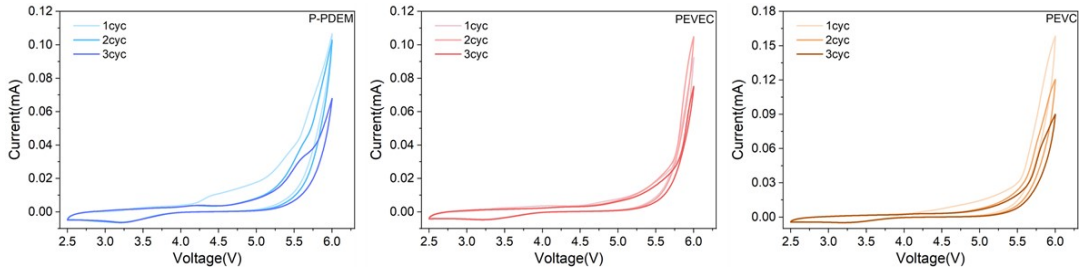

Fig.S8 CV curves using Li/SS cells at a scan rate of 0.1 mV s^{-1} of P-PDEM, PEVEC and PEVC electrolytes.

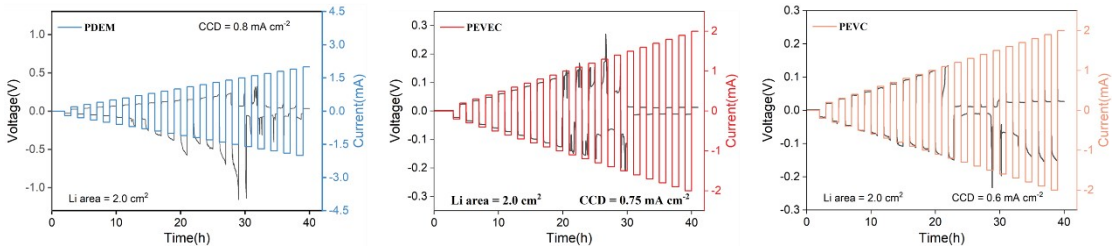

Fig.S9 Comparison of polarization voltages of Li/Li symmetrical batteries with P-PDEM, PEVC and PEVEC electrolytes.

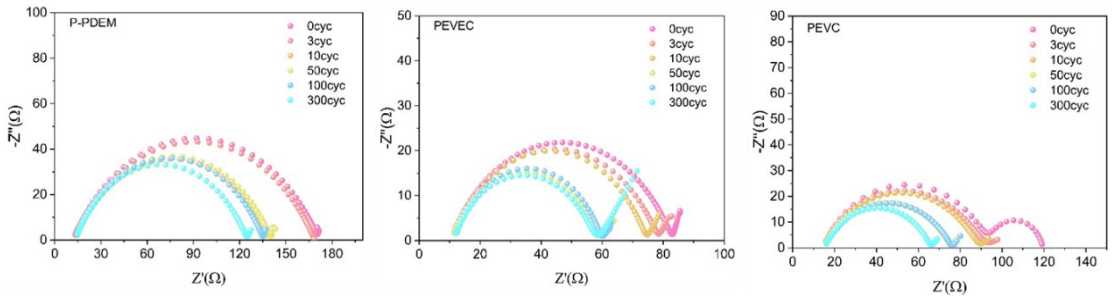

Fig.S10 The impedance of Li/P-PDEM/Li, Li/PEVEC/Li and Li/PEVC /Li battery after different cycles.

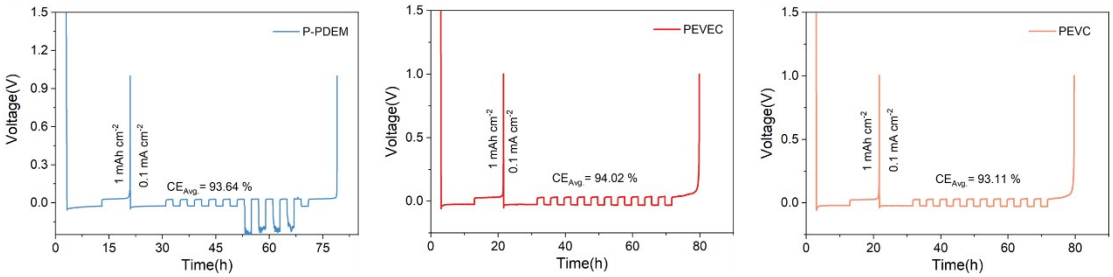

Fig.S11 Coulombic efficiency test of Li/Cu cells. (0.1 mA cm^{-2} with a capacity of 0.1 mAh cm^{-2}).

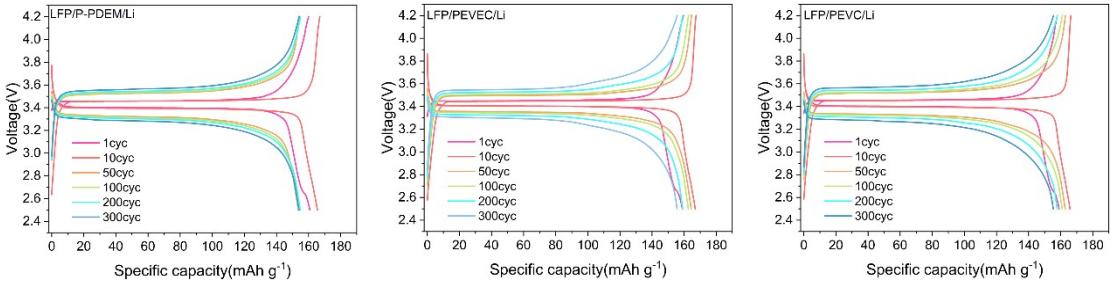

Fig.S12 Charge- discharge profiles and cycling performance of Li/LFP cells with three electrolytes at 25 °C.

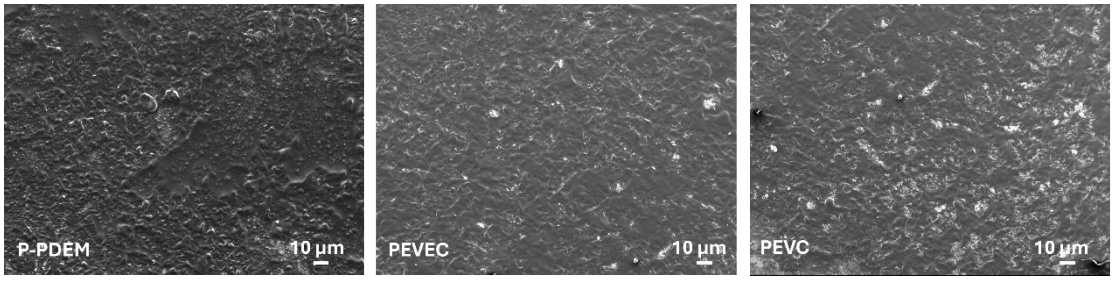

Fig.S13 SEM image of LFP cathode after 650 cycles of Li/LFP battery.

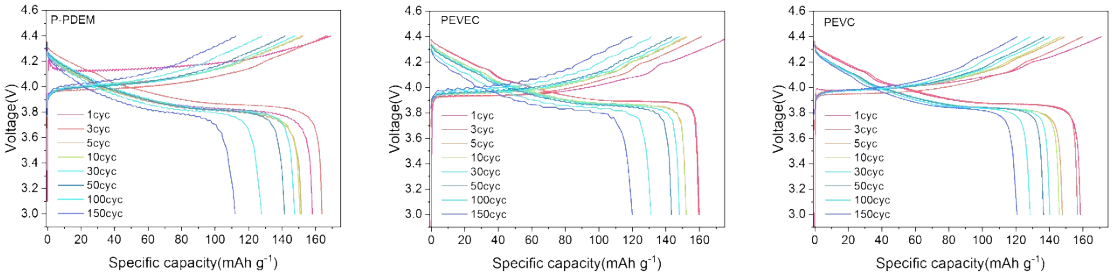

Fig.S14 Charge- discharge profiles and cycling performance of Li/LCO cells with three electrolytes at 25 °C.

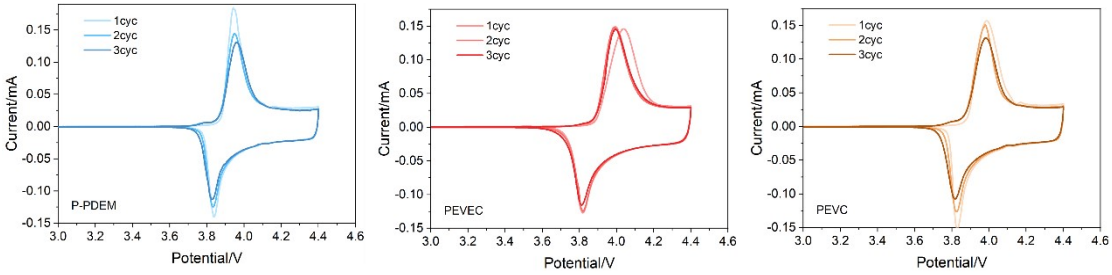

Fig.S15 CV curves using Li/LCO cells at a scan rate of 0.038 mV s^{-1} of P-PDEM, PEVEC and PEVC electrolytes.

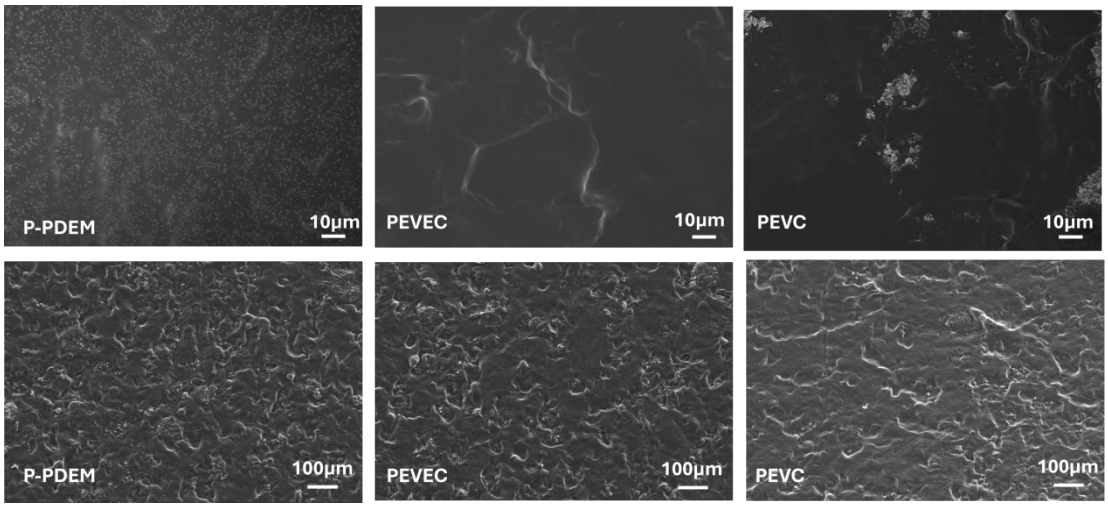

Fig.S16 SEM image of lithium metal anode (top) and LCO cathode (bottom) after 150 cycles of Li/LCO battery.

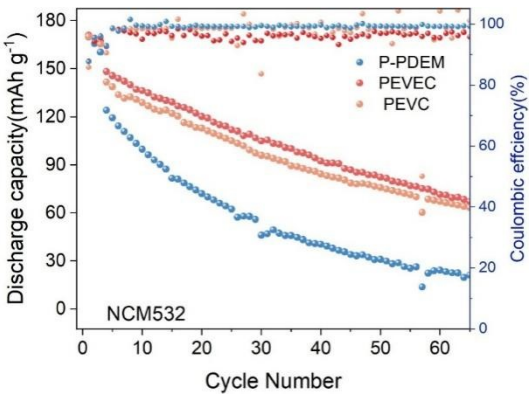

Fig.S17 Cycle stability of Li/NCM532 battery at 25 °C.

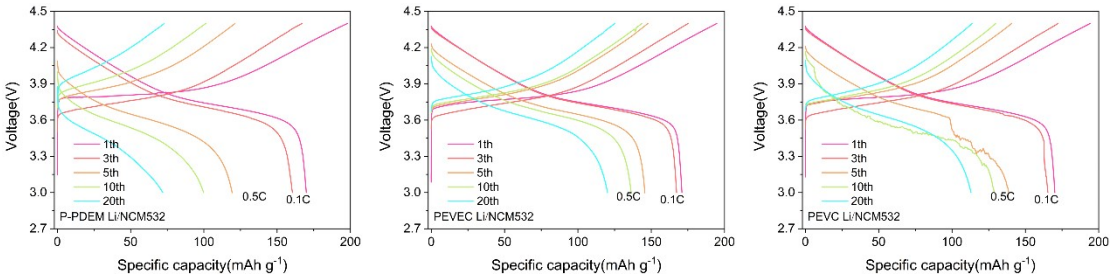

Fig.S18 Charge- discharge profiles and cycling performance of Li/NCM532 cells with three electrolytes at 25 °C.

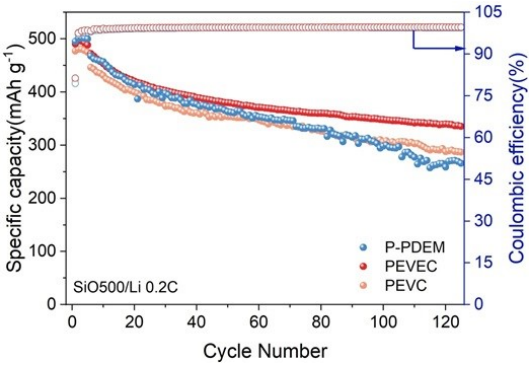

Fig.S19 Long-cycle performance of SiO500/Li cells.

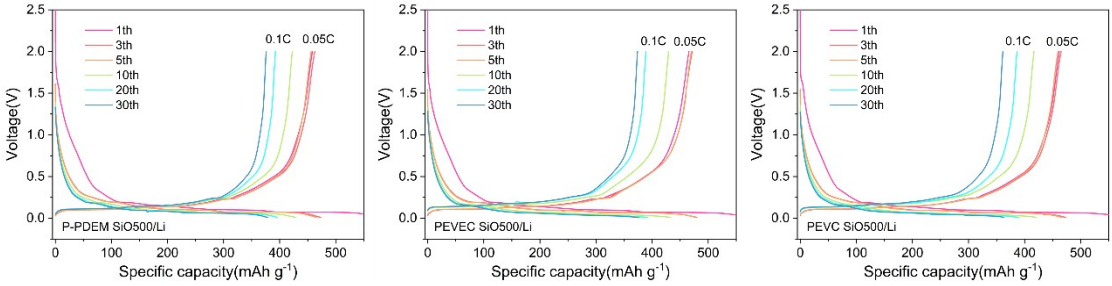

Fig.S20 Capacity-voltage profile of SiO500/Li battery.

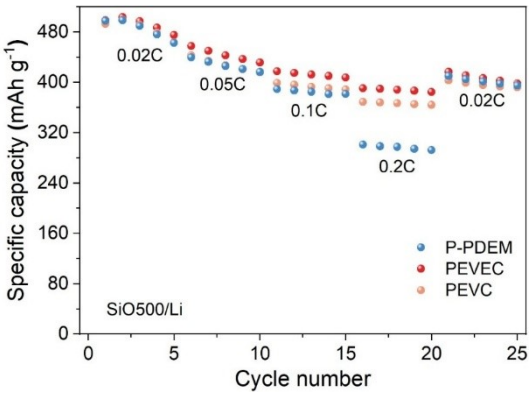

Fig.S21 Rate capability of SiO500/Li cell.

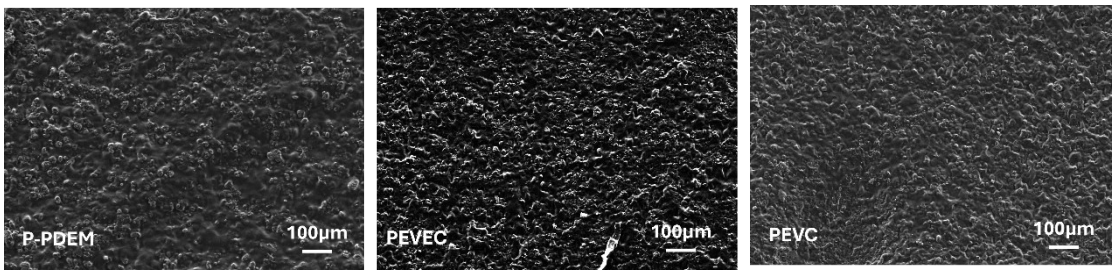

Fig.S22 SEM image of SiO500 anode after 200 cycles of SiO500/Li battery.

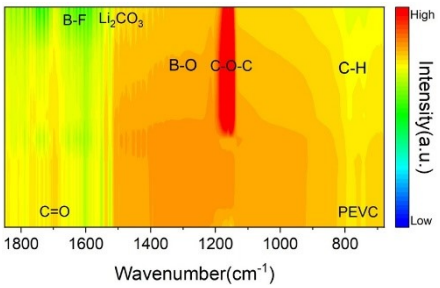

Fig.S23 In-situ infrared spectra of electrolyte PEVC.

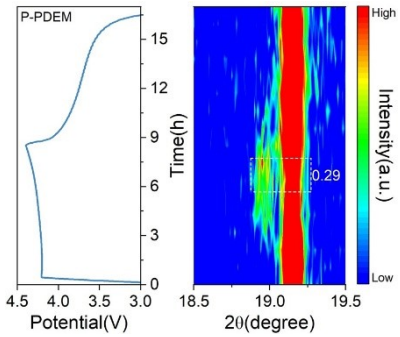

Fig.S24 In-situ XRD patterns of P-PDEM electrolytes.

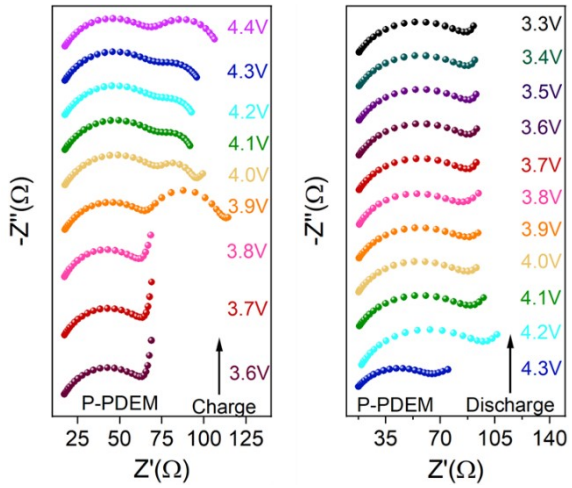

Fig.S25 In-situ impedance spectrum of the battery during the charge-discharge process with the P-PDEM electrolyte.

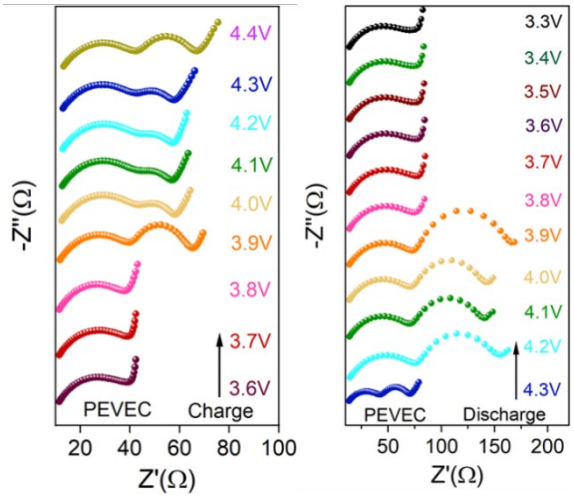

Fig.S26 In-situ impedance spectrum of the battery during the charge-discharge process with the PEVEC electrolyte.

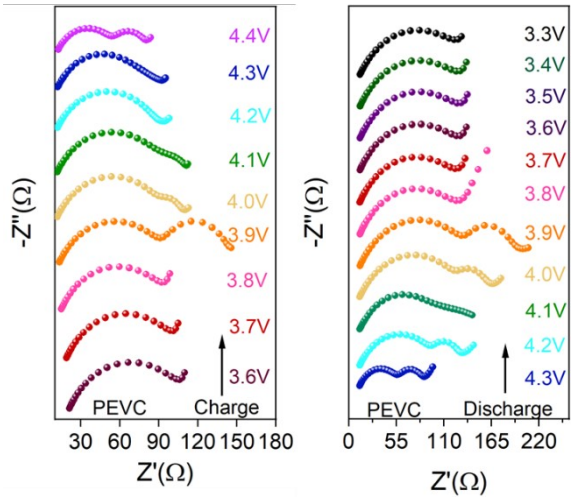

Fig.S27 In-situ impedance spectrum of the battery during the charge-discharge process with the PEVC electrolyte.

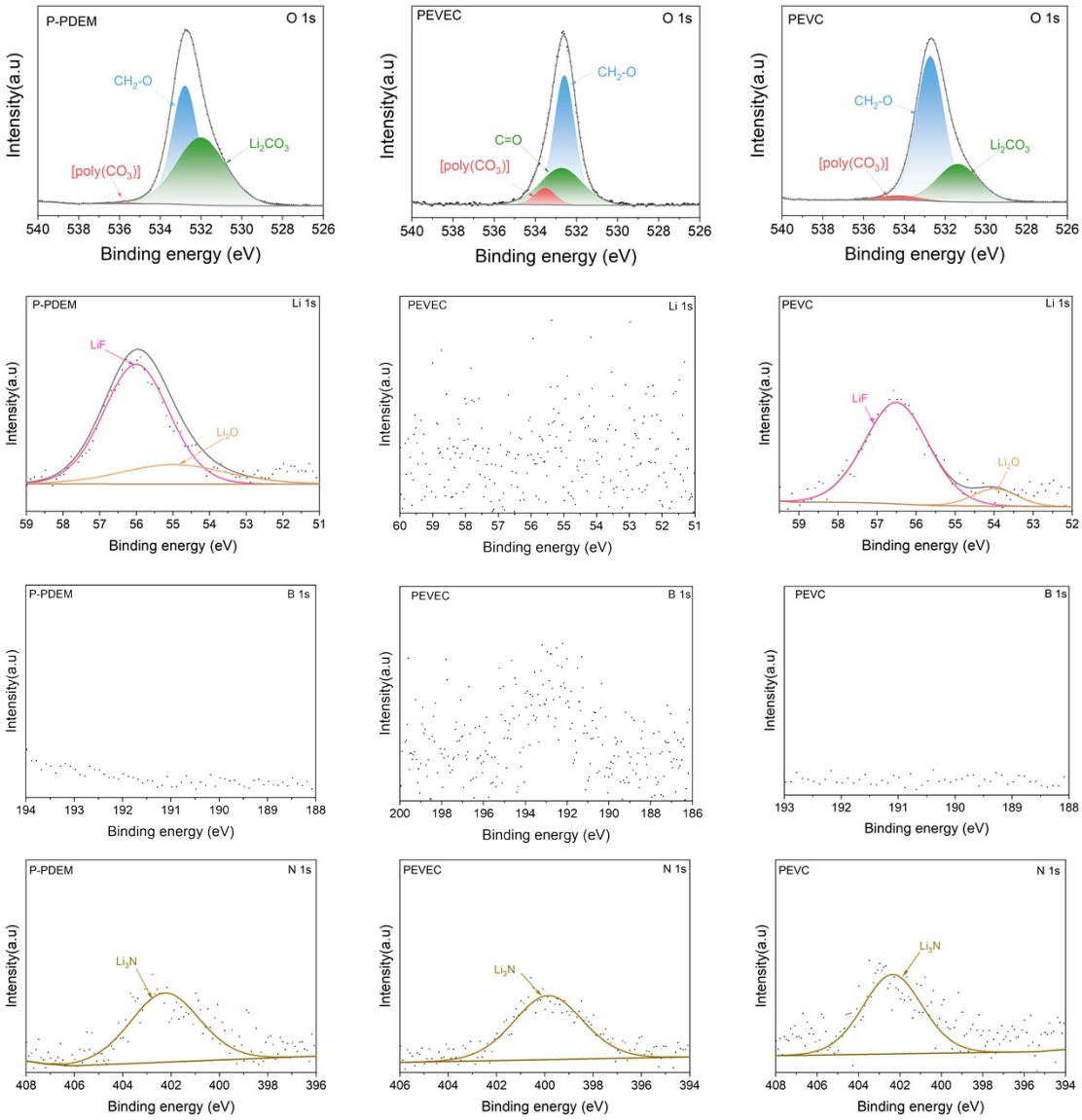

Fig.S28 XPS curves of O1s, Li1s, N1s and B1s in lithium metal anode of a Li/LCO battery with 100 cycles of P-PDEM, PEVEC and PEVC polymer electrolytes.

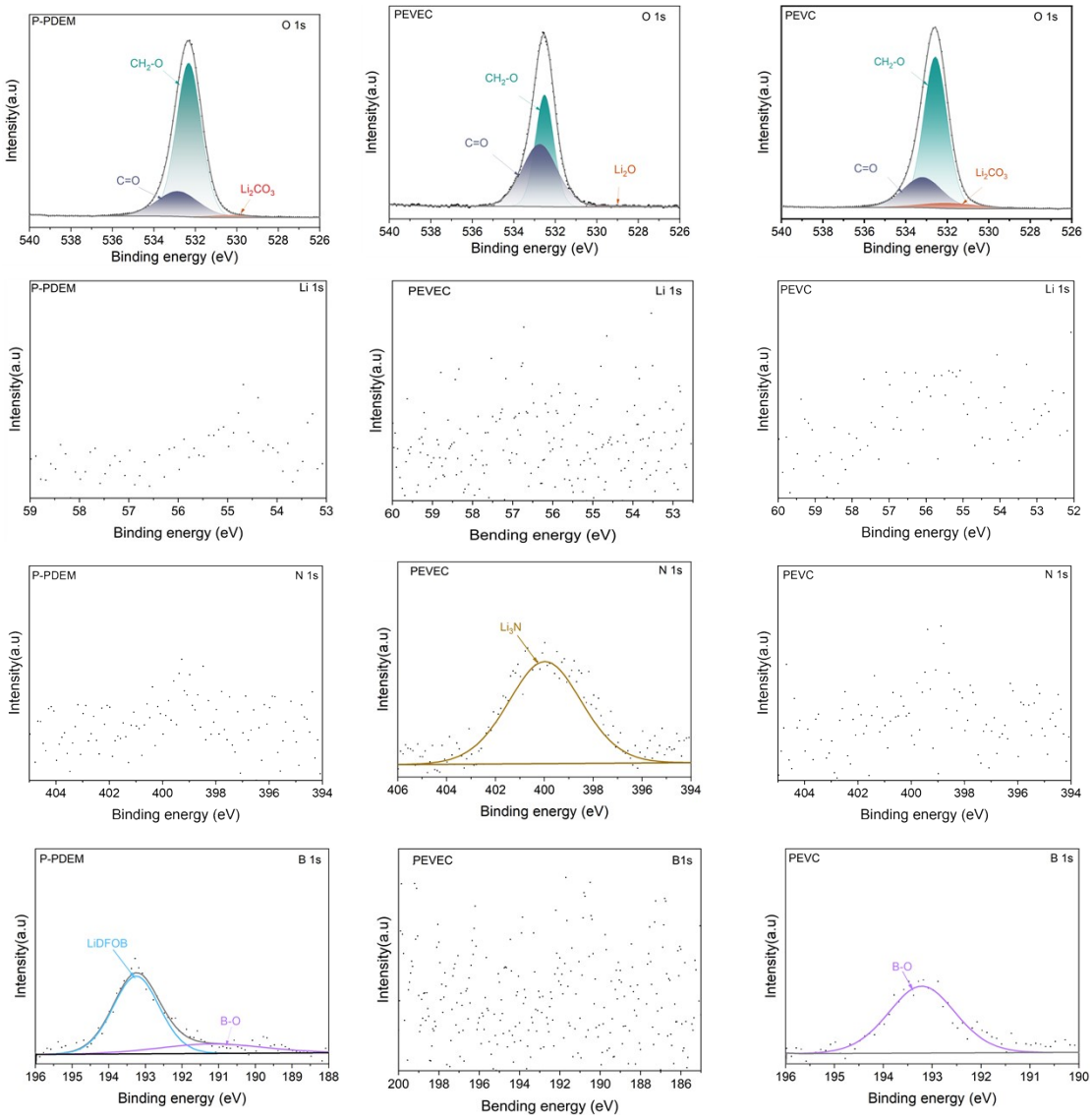

Fig.S29 XPS curves of O1s, Li1s, N1s and B1s in LCO cathode of a Li /LCO battery with 100 cycles of P-PDEM, PEVEC and PEVC polymer electrolytes.

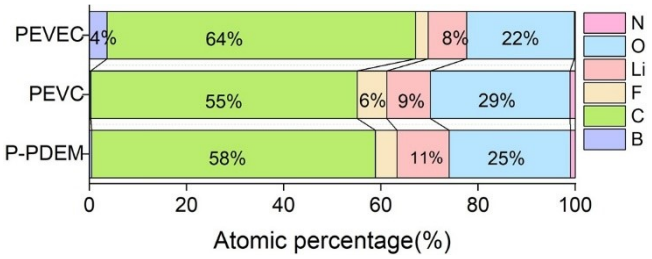

Fig.S30 Atomic ratios of SEI films correspond to XPS spectra in P-PDEM, PEVEC, and PEVC.

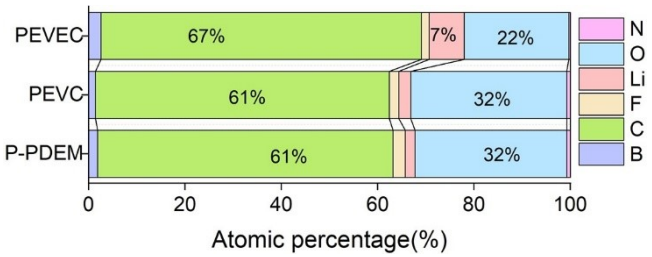

Fig.S31 Atomic ratios of CEI films correspond to XPS spectra in P-PDEM, PEVEC, and PEVC.

3. Supporting Tables

Table S1. Impedance values of PEVEC, PEVC, and P-PDEM electrolytes after different cycle numbers.

Electrolyte system	**PEVEC**			**PEVC**			**P-PDEM**		
Cycle number	**R_b (Ω)**	**R_{SEI} (Ω)**	**R_{ct} (Ω)**	**R_b (Ω)**	**R_{SEI} (Ω)**	**R_{ct} (Ω)**	**Rb (Ω)**	**R_{SEI} (Ω)**	**R_{ct} (Ω)**
0	11.15	7.85	62.56	14.55	79.71	24.47	12.88	24.80	129.7
3	11.39	6.81	58.70	15.69	14.6	52.14	13.57	21.20	130.0
10	11.89	5.86	55.32	15.16	6.07	69.03	13.89	19.54	101.1
50	11.31	6.15	40.19	15.85	7.90	49.94	14.08	18.49	105.7
100	12.24	4.01	42.66	16.09	7.17	50.76	14.09	24.12	94.09
300	11.77	3.20	42.51	15.9	5.487	42.91	14.16	21.65	86.52

Table S2. In-situ impedance values of the battery during charge-discharge with PEVC electrolyte.

Voltage rises	**OCV**	**3.6 V**	**3.7 V**	**3.8 V**	**3.9 V**	**4.0 V**	**4.1 V**	**4.2 V**	**4.3 V**	**4.4 V**
R_b (Ω)	--	20.88	18.88	14.97	12.76	10.95	10.95	10.94	11.22	11.96
R_{SEI} (Ω)	--	4.565	6	6.909	84.95	86.46	86.08	4.458	51.66	45.33
R_{ct} (Ω)	--	85.04	79.86	68.51	43.03	6.11	10.42	75.88	33.88	22.31
Voltage drops	**3.5V**	**3.6 V**	**3.7 V**	**3.8 V**	**3.9 V**	**4.0 V**	**4.1 V**	**4.2 V**	**4.3 V**	**4.4 V**
R_b (Ω)	13.17	11.68	12.87	11.33	11.88	11.59	11.87	11.93	12.11	11.96
R_{SEI} (Ω)	89.84	77.0	92.42	124.9	135.3	122.3	103.9	93.38	47.83	45.33
R_{ct} (Ω)	6.146	63.17	6.1	21.5	24.18	37.79	20.0	13.57	25.93	22.31

Table S3. In-situ impedance values of the battery during charge-discharge with PEVEC electrolyte.

Voltage rises	**OCV**	**3.6 V**	**3.7 V**	**3.8 V**	**3.9 V**	**4.0 V**	**4.1 V**	**4.2 V**	**4.3 V**	**4.4 V**
R_b (Ω)	--	10.74	10.32	10.22	10.57	10.98	11.14	11.28	11.3	11.43
R_{SEI} (Ω)	--	1.562	0.9005	31.22	33.44	35.14	34.2	34.33	33.93	34.71
R_{ct} (Ω)	--	32.28	34.57	2.177	16.96	12.04	12.15	12.75	12.28	20.02
Voltage drops	**3.4V**	**3.5V**	**3.6 V**	**3.7 V**	**3.8 V**	**3.9 V**	**4.0 V**	**4.1 V**	**4.2 V**	**4.3 V**
R_b (Ω)	13.26	13.23	13.2	11.8	13.28	11.64	11.54	11.64	12.08	11.52
R_{SEI} (Ω)	8.186	8.092	7.905	30.55	10.54	66.02	65.75	65.06	70.2	34.98
R_{ct} (Ω)	48.22	49.59	50.92	53.4	46.73	95.79	62.82	61.7	68.43	23.57

Table S4. In-situ impedance values of the battery during charge-discharge with P-PDEM electrolyte.

Voltage rises	**OCV**	**3.6 V**	**3.7 V**	**3.8 V**	**3.9 V**	**4.0 V**	**4.1 V**	**4.2 V**	**4.3 V**	**4.4 V**
R_b (Ω)	--	16.07	15.96	17.00	16.67	16.54	16.43	16.4	16.37	16.43
R_{SEI} (Ω)	--	25.05	9.24	4.948	54.01	61.39	61.46	60.96	59.69	56.92
R_{ct} (Ω)	--	18.8	46.82	39.64	37.87	15.64	13.18	13.32	17.39	31.14
Voltage drops	**3.4V**	**3.5V**	**3.6 V**	**3.7 V**	**3.8 V**	**3.9 V**	**4.0 V**	**4.1 V**	**4.2 V**	**4.3 V**
R_b (Ω)	17.00	16.5	16.62	17.65	17.59	17.93	17.81	18.08	19.25	16.4
R_{SEI} (Ω)	70.69	49.32	53.75	6.426	51.4	47.56	44.88	48.3	57.95	53.51
R_{ct} (Ω)	6.00	18.09	14.26	60.27	12.59	3.756	5.274	3.838	3.321	34.32

Table S5. Comparison of Li/LFP cell performance in this work with typical solid electrolytes in literature.

Electrolytes	Temperature (°C)	Rate	Cycle	Capacity retention rate (%)	Ref.
PNPU/PVDF-HFP	30	0.2	300	90	[1]
PAN/LLZTO	60	0.5	190	93.6	[2]
PEO/SN/MOF framework	55	0.5	600	85.7	[3]
PEO/ Ca-PO_4-CO_3 nanowires	60	0.2	450	98	[4]
PVDF/PPC	30	0.2	100	69.2	[5]
PVDF/h-BN nanosheets	60	0.2	170	96	[6]
PVDF-HFP/LALZO/ h-BN	55	0.2	100	92	[7]
PEO/Aramid nanofibers	60	0.1	180	78	[8]
PEGMA/3-BMP	60	0.1	60	94.5	[9]
PVDF/SiO_2/LLTO	25	0.5	100	95	[10]
PAN/ZIF-8 nanofiber	25	2	500	86.66	[11]
PMBA/GF/DEE	30	1	600	83.7	[12]
PL/LILZO nanofibers	60	0.5	400	80	[13]
PEO/MEMO/LLZTO-	60	1	200	90.9	[14]
This work	25	0.5	1000	93.73	

4. Supporting Videos

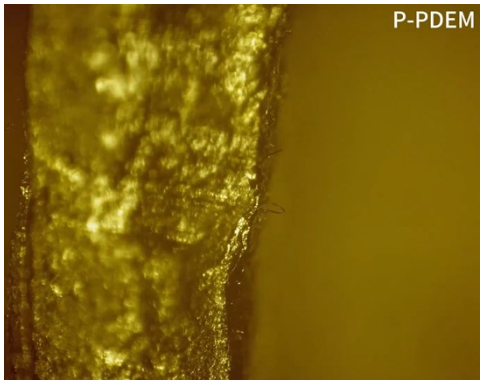

Video S1. Video (accelerated 100x) showing the stripping process of a Li/Li battery in PEVEC electrolyte under a 90 µA current.

Video S2. Video (accelerated 100x) showing the stripping process of a Li/Li battery in PEVEC electrolyte under a 90 µA current.

Video S3. Video (accelerated 100x) showing the stripping process of a Li/Li battery in PEVEC electrolyte under a 90 µA current.

Video S4. Pouch cell puncture test.

Video S5. Pouch cell squeeze test.

5. References

1. Y. Ye, X. Zhu, N. Meng and F. Lian, *Advanced Functional Materials*, 2023, **33**, 2307045.
2. N. Chen, B. Gui, B. Yang, C. Deng, Y. Liang, F. Zhang, B. Li, W. Sun, F. Wu and R. Chen, *Small*, 2023, **20**, 2305576.
3. S. Guo, Y. Su, K. Yan, C. Zhao, Y. Lu, H. Wang, J. Dong, N. Li, Y. Liu, Y. Guan, F. Wu and L. Chen, *Advanced Science*, 2024, **11**, 2404307.
4. L. Yang, H. Zhang, H. Xu, W. Peng, L. Wu, Y. Cheng, Y. Liu, L. Xu and L. Mai, *Advanced Energy Materials*, 2024, **14**, 2401829.
5. Z. Jia, M. Jia, Q. Sun, N. Wang, Z. Bi and X. Guo, *Energy Storage Materials*, 2024, **68**, 103325.
6. Y. Zhao, Y. Qin, X. Da, X. Weng, Y. Gao, G. Gao, Y. Su and S. Ding, *ChemSusChem*, 2022, **15**, e202201554.
7. J.-H. Kim, D.-H. Park, J.-S. Jang, J.-H. Shin, M.-C. Kim, S.-B. Kim, S.-H. Moon, S.-N. Lee and K.-W. Park, *Chemical Engineering Journal*, 2022, **446**, 137035.
8. L. Liu, R. Xu, J. Tu, R. Zhou, J. Mo, T. Yang, Q. Zhao, M. Zhang, D. Zhang and M. Li, *The Journal of Physical Chemistry C*, 2025, **129**, 6138-6147.
9. T. Wang, Y. Tong, Q. B. Li, T. Xu, W. Jin, D. Zhou and Z. Zhang, *ACS Applied Polymer Materials*, 2025, **7**, 2933-2944.
10. G. Zheng, Y. Chen, R. Chen, X. Li, Z. Chen, Z. Zeng and H. Yan, *Chemical Engineering Journal*, 2025, **518**, 164616.
11. J. Gao, Y. Chai, J. Ni, Y. Zeng, G. Zhang, X. Liu, D. Ning, X. Jin, H. Zhao, D. Zhou, R. Gao, W. Wu, J. Wang and Y. Li, *Chemical Engineering Journal*, 2025, **512**, 162738.
12. Y. Zhang, S. Lu, Z. Zhao, X. Zhang, H. Lv, Z. Yang, W. Sun, M. Xie and D. Mu, *Chemical Engineering Journal*, 2024, **487**, 150474.
13. Y. Teng, H. Liu, Q. Wang, Y. He, Y. Hua, C. Li and J. Bai, *Journal of Energy Storage*, 2024, **76**, 109784.
14. T. Duan, H. Cheng, Y. Liu, Q. Sun, W. Nie, X. Lu, P. Dong and M.-K. Song, *Energy Storage Materials*, 2024, **65**, 103091.